NOMA-Based Statistical Signal Transmission for Beyond 5G Communications

Tianheng Xu[1,2], Ning Zhang[3], Ting Zhou[1,2(✉)], Honglin Hu[1], and Xiaoming Tao[4]

[1] Shanghai Advanced Research Institute, Chinese Academy of Sciences, Shanghai, China
{xuth,zhouting,huhl}@sari.ac.cn
[2] Shanghai Frontier Innovation Research Institute, Shanghai, China
[3] Department of Electrical and Computing Engineering, University of Windsor, Windsor, ON, Canada
ning.zhang@uwindsor.ca
[4] Department of Electronic Engineering, Tsinghua University, Beijing, China
taoxm@tsinghua.edu.cn

Abstract. With the rollout of fifth-generation (5G) communications, researches for beyond fifth generation (B5G) communications are being launched globally. In this paper, we explore for possible ways to integrate two promising techniques, including non-orthogonal multiple access (NOMA) and statistical signal transmission (SST), seeking a feasible perspective to promote the development of B5G communications. Specifically, NOMA allows multiple users to occupy the same spectrum resource, which can greatly improve spectrum efficiency. On the other hand, SST utilizes higher-order moments to convey additional data over traditional first-order moment signals, which is capable of supporting inter-system data exchange. To verify the feasibility of combining NOMA and SST, in this paper we outline the transceiver architecture, and conceive the workflow for this promising NOMA-SST system. Considering that NOMA users at a same spectrum resource have intrinsic energy gaps, we further design a dedicated transmission strategy for NOMA-SST technique, aiming at compensating the performance for NOMA users with lower power levels. Numerical results reflect that the proposed technique can achieve satisfactory detection performance, which is promising for applications.

Keywords: NOMA · Beyond 5G · Spectrum efficiency · Statistical signal transmission · Differential window integration

1 Introduction

Wireless communication technologies have experienced incredible growth in the past decades. Now the human society has already initiated a global fifth-generation (5G) communication era [1–5]. Currently, the wireless communication community

C. T. Calafate et al. (Eds.): MONAMI 2021, LNICST 418, pp. 282–298, 2022.
https://doi.org/10.1007/978-3-030-94763-7_22

starts to research the beyond fifth generation (B5G) communication systems [6–8]. B5G is envisioned as a multifarious ecosystem, which contains multi-type subsystems, large amount of different applications and diversified services [9–11]. Accordingly, how to (i) effectively support the accompanying tremendous data in B5G ecosystem [12,13], while (ii) maintaining efficient collaborations among different systems and applications [14–16], becomes a critical challenge.

Non-orthogonal multiple access (NOMA) technique is regarded as an enabling technique for B5G systems [17–19]. Relying on the aid of successive interference cancellation (SIC), NOMA allows multiple users to occupy the same spectrum resource. Lots of studies have proved that NOMA outperforms traditional orthogonal multiple access from multiple aspects, especially in spectrum efficiency [20–22]. On the other hand, statistical signal transmission (SST) is another emerging technique, which can deliver additional data streams over regular signals. The SST data stream is formed in the shape of higher-order moments, it neither affects the transmission performance; nor causes extra spectrum sacrifice from the underlying regular signals (in first-order moment) [23,24]. Moreover, SST is also easy to be implemented and is compatible with common communication systems [25,26]. Therefore, SST can facilitate efficient collaborations among different subsystems and applications for future B5G ecosystem.

Referring to the advantages of the two techniques above, we imagine that if NOMA and SST can be well merged: (i) spectrum efficiency can be doubly refined, thus the huge wireless traffic burden will be alleviated; (ii) efficient collaborations among systems and applications will be facilitated. Accordingly, the union technique of NOMA-SST has the potential to promote a smooth evolution from 5G to B5G. However, existing literature still lacks the answer of whether NOMA and SST can work together. To answer this question, in this paper, we probe for possible ways to combine NOMA and SST. Particularly, the major contributions can be summarized as follows.

- First, we analyze the working principles of both NOMA and SST, then we outline the preliminary transceiver architecture for the union technique of NOMA-SST.
- Second, based on the transceiver architecture, we further conceive the operational workflow for NOMA-SST technique.
- Third, considering that NOMA users at the same spectrum resource have intrinsic energy gaps, we dedicatedly design an enhanced transmission strategy to compensate the weaker users.
- Forth, we provide numerical results and demonstrate that the proposed NOMA-SST technique has satisfactory detection performance.

The reminder of this paper can be organized as follows. First in Sect. 2, we design the transceiver architecture and detection workflow for NOMA-SST technique. The properties of the proposed technique are discussed as well. Then in Sect. 3, we provide the differential window integration strategy to further strengthen the ability of NOMA-SST technique. Section 4 showcases simulation results to verify the performance of the proposed technique. Finally, our work of this paper is concluded in Sect. 5.

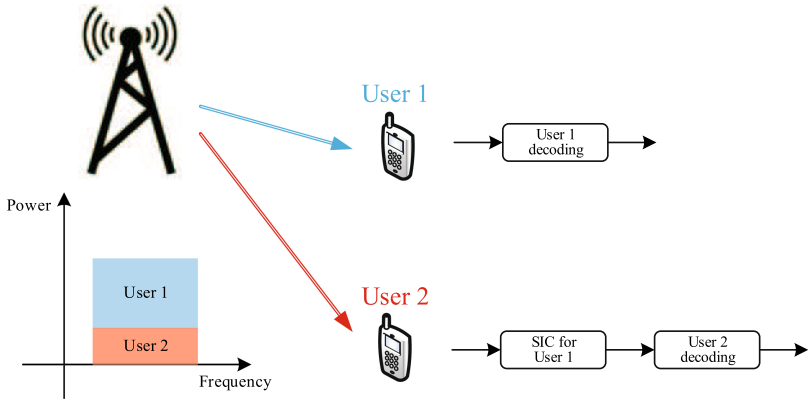

Fig. 1. Downlink NOMA scenario with two users.

2 System Design

NOMA technologies usually exploit power level difference for multiple users to occupy the same spectrum resource [27,28]. Figure 1 illustrates an example of a typical downlink NOMA scenario with two users. The two users are transmitting data on the same spectrum resource. Specifically, User 1 has higher power level than User 2. Since the distinct power level difference, the data of User 1 can be directly detected at the receiver of User 1, while the data of User 2 is regarded as a part of noise. On the other hand, for the receiver of User 2: when receiving the mixed signals, the SIC mechanism first decodes data of User 1; after that, the receiver of User 2 subtracts the content of User 1's data, then successively decodes data of User 2 [29,30].

2.1 Transceiver Architecture Design

Based on the typical NOMA scenario above, we design the transceiver architecture for NOMA-SST, as Fig. 2 shows. At the transmitter, the SST-data of one user (User 1 or User 2), which is performed in the form of high order moment, is embedded into the first order moment of traditional frequency data. Thus, the two kinds of data streams of one user (User 1 or User 2) are combined into the same physical stream. After that, referring to the power level difference, the two users' physical streams further mix together. At last, four paralleled data streams are transmitted at the same band.

Without loss of generality, in this paper we adopt a classical two-antenna transmitting configuration [31]. The detailed operational principle of NOMA-SST can be elaborated as follows. SST signal is produced by a cyclic delay diversity [32,33] based orthogonal frequency division multiplexing (OFDM) system. Before transmitting, the SST data is mapped into a dynamic cyclic delay sequence. Then during the transmission, the first transmitting antenna (antenna-A) sends typical OFDM symbols; at the same time, such symbols are cyclically

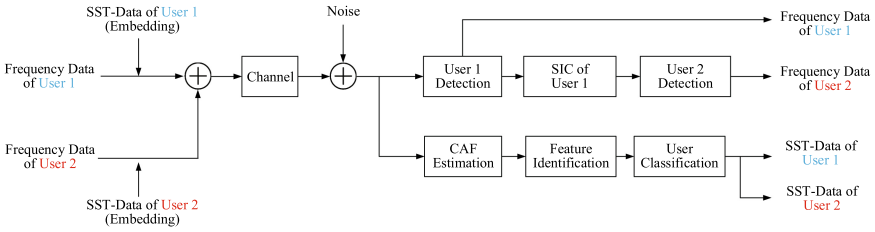

Fig. 2. Transceiver architecture of downlink NOMA-SST technique.

shifted according to the aforementioned dynamic cyclic delay sequence, and sent by the second transmitting antenna (antenna-B). Therefore, SST data is embedded into the frequency data. This implementation does not induce extra bandwidth cost. Particularly, the signal sent by antenna-A can be written as

$$s_A(n) = \sqrt{P_1} s_{1,A}(n) + \sqrt{P_2} s_{2,A}(n), \tag{1}$$

where P_1 and P_2 are transmitting power of User 1 and User 2, respectively. We set User 1 has the higher power level than User 2, thus $P_1 > P_2$. The signal components

$$s_{1,A}(n) = \frac{1}{\sqrt{2N}} \sum_{l=-\infty}^{+\infty} g(n - lM) \sum_{k=0}^{N-1} \alpha_{l,k} W_N^{k[(l+1)M-n]} \tag{2}$$

and

$$s_{2,A}(n) = \frac{1}{\sqrt{2N}} \sum_{l=-\infty}^{+\infty} g(n - lM) \sum_{k=0}^{N-1} \beta_{l,k} W_N^{k[(l+1)M-n]} \tag{3}$$

belong to User 1 and User 2, respectively. In (2) and (3), N is the Fast Fourier Transform size, $M = N+$ cyclic prefix length. $W_N = e^{\frac{-j2\pi}{N}}$, α and β are OFDM data from User 1 and User 2, respectively. l and k denote sequence number of symbol and subcarrier of OFDM signal, respectively. $g(n)$ is the window function, which can be expressed as

$$g(n) = \begin{cases} 1, & n \in [0, M-1], \\ 0, & \text{otherwise.} \end{cases} \tag{4}$$

Antenna-B sends the identical data as that in antenna-A, but the data should be cyclically shifted before transmitting, which can be expressed as

$$s_B(n) = \sqrt{P_1} s_{1,B}(n) + \sqrt{P_2} s_{2,B}(n), \tag{5}$$

with

$$s_{1,B}(n) = \frac{1}{\sqrt{2N}} \sum_{l=-\infty}^{+\infty} g(n - lM) \sum_{k=0}^{N-1} \alpha_{l,k} W_N^{k[(l+1)M-n]} W_N^{k\Delta} \tag{6}$$

and

$$s_{2,B}(n) = \frac{1}{\sqrt{2N}} \sum_{l=-\infty}^{+\infty} g(n - lM) \sum_{k=0}^{N-1} \beta_{l,k} W_N^{k[(l+1)M-n]} W_N^{k\bar{\Delta}}. \tag{7}$$

In (6) and (7), $s_{1,B}$ and $s_{2,B}$ are shifted signal components from User 1 and User 2, respectively. Δ and $\bar{\Delta}$ are cyclic delays, which are extracted from User 1 and User 2's dynamic cyclic sequences, respectively. The final transmitted signals can then be represented as

$$\mathbf{S}(n) = \begin{bmatrix} s_A(n) \\ s_B(n) \end{bmatrix}. \tag{8}$$

2.2 Detection Work Flow Design

In this subsection, we elaborate the detection work flow. The received signal can be written as

$$r(n) = \mathbf{h}\mathbf{S}(n) + v(n), \tag{9}$$

where $v(n)$ denotes the additive white Gaussian noise, $\mathbf{h}$ represents the channel gain, and we have

$$\mathbf{h} = [h_A, h_B]. \tag{10}$$

Referring to Fig. 2, when the receiver gets the signal, the processing modules of frequency domain and SST domain work in parallel. For the frequency domain, it first regards User 2's data as a part of noise, and directly detects User 1's data. After getting User 1's reconstructed data, the SIC process subtracts it from the mixed signal, and then detects User 2's data. Since the NOMA detection process in frequency domain has been well studied in lot of researches, the follow-up details are omitted in this paper.

On the other hand, the SST module works simultaneously in the frequency domain. In particular, it contains three submodules:

- Cyclic autocorrelation function (CAF) estimation;
- Feature identification;
- User classification.

CAF estimation is the first step of SST detection. Notice that manmade signals are mostly cyclostationary random processes [34]. Hence a signal stream' CAF can be represented as waveforms in a three-dimensional coordinate system. Such a coordinate system is usually established by lag parameter, cyclic frequency parameter, and coherence energy value [35,36]. Based on this theory, CAF estimation submodule extracts the peak information of CAF waveforms from the mixed signal. Given L as observation window length of symbol unit, the value of CAF can be estimated as

$$C^{(L)}(b, \tau) = \frac{1}{LM} \sum_{n=0}^{LM-1} r(n) r^*(n + \tau) W_M^{bn}, \tag{11}$$

where $\tau \in [1, M]$ and $b \in [1, M]$ are lag parameter and cyclic frequency parameter, respectively.

After obtaining CAF value, the feature identification submodule exploits a multiple hypothesis test to operate the detection process. Note that cyclic delays have the symmetric property [24], for one user there are $N/2$ distinct SST features in an N-subcarrier system. To avoid conflicts, we set $\Delta \neq \bar{\Delta}$. Hence, for each hypothesis we have

$$H_{\Delta}: \begin{cases} C^{(L)}(b,\Delta) & = \tilde{C}^{(L)}(b,\Delta) + \varepsilon_r^{(L)}(b,\Delta) \\ C^{(L)}(b,\tau) & = \varepsilon_r^{(L)}(b,\tau) \end{cases} \quad \text{for} \quad \tau \in (1,2,\cdots,N/2),\ \tau \neq \Delta, \tag{12}$$

$$H_{\bar{\Delta}}: \begin{cases} C^{(L)}\left(b,\bar{\Delta}\right) & = \tilde{C}^{(L)}\left(b,\bar{\Delta}\right) + \varepsilon_r^{(L)}\left(b,\bar{\Delta}\right) \\ C^{(L)}(b,\tau) & = \varepsilon_r^{(L)}(b,\tau) \end{cases} \quad \text{for} \quad \tau \in (1,2,\cdots,N/2),\ \tau \neq \bar{\Delta}, \tag{13}$$

and

$$\begin{aligned} H_j : C^{(L)}(b,\tau) &= {C_v}^{(L)}(b,\tau) \\ &= \frac{1}{LM}\sum_{n=0}^{LM-1} v(n)v^*(n+\tau)W_M^{bn} \\ &\quad \text{for} \quad \tau \in (1,2,\cdots,N/2), \end{aligned} \tag{14}$$

where $j \in \left(1,2,\cdots,\frac{N}{2}\right)$ and $j \neq \{\Delta,\bar{\Delta}\}$; $\tilde{C}^{(L)}$, ${C_v}^{(L)}$ and $\varepsilon_r^{(L)}$ are symbol coherency components, noise coherency components and unrelated coherency components within observation window length L, respectively.

Next, the user classification submodule could extract a local two-dimensional CAF value from the entire three-dimensional coordinate system, and classify the locations of two users' feature peaks. Here we take the CAF value at $b = M$ as an example, and the local feature peaks can then be presented as

$$\Gamma^{(L)}(\tau) = \left|C^{(L)}(M,\tau)\right|. \quad \text{for} \quad \tau \in (1,2,\cdots,N/2) \tag{15}$$

Given available feature location sets as

$$\Omega = \{1,2,\cdots,N/2\} \tag{16}$$

and

$$\bar{\Omega} = \Omega - \{\Delta\}, \tag{17}$$

respectively. The classification processes for User 1 and User 2 can be performed as

$$\Delta = \arg \max_{\tau \in \Omega} \Gamma^{(L)}(\tau) \tag{18}$$

and

$$\bar{\Delta} = \arg \max_{\tau \in \bar{\Omega}} \Gamma^{(L)}(\tau), \tag{19}$$

respectively.

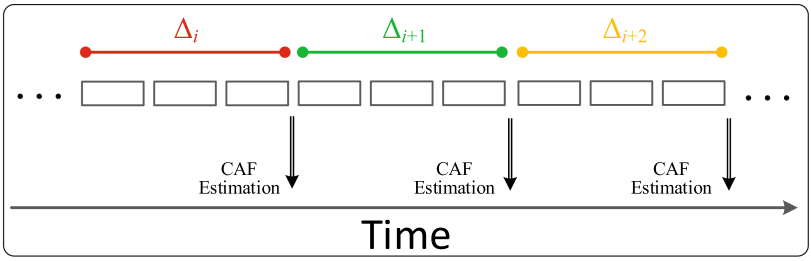

(a) A classical SST scheme.

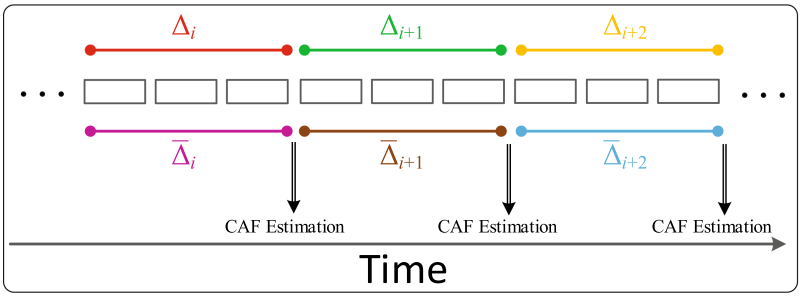

(b) A default NOMA-SST scheme.

Fig. 3. Detection workflow comparison between SST and NOMA-SST schemes. Boxes represent OFDM symbols in time domain, different color coverages indicate different cyclic delay ranges.

To visualize the difference between SST and NOMA-SST, Figs. 3 and 4 exhibit detection workflow comparison and feature comparison between SST and NOMA-SST schemes, respectively. In particular, Fig. 3(a) illustrates a classical SST scheme. In this case, every moment there is always one unique cyclic delay state (i.e. Δ_i series). The detection process is essentially a single-pole feature identification problem, which can be reflected in Fig. 4(a). While in a default NOMA-SST case as Fig. 3(b) shows, multiple cyclic delay states (belonging to different NOMA users) coexist and overlap with each other (i.e. Δ_i series and $\bar{\Delta}_i$ series). The detection process becomes a multi-pole feature identification problem. We can perceive such a phenomenon in Fig. 4(b). Fortunately, although the CAF estimation processes are simultaneously implemented for different NOMA users, their SST features can be easily distinguished owing to the power level gap.

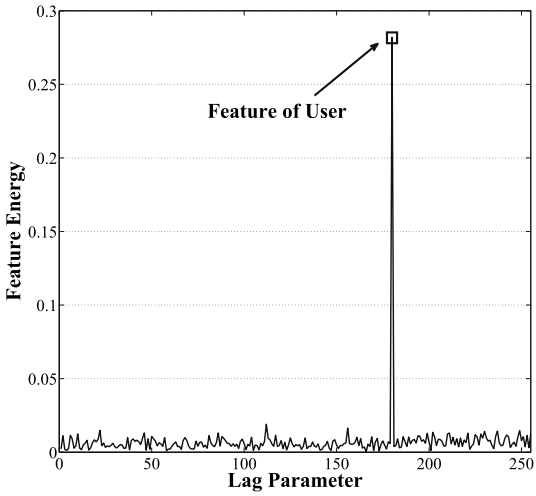

(a) A classical SST scheme.

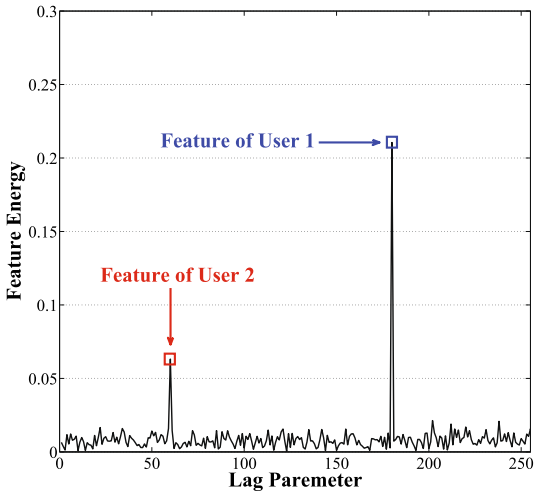

(b) A default NOMA-SST scheme with $P_1 = 4P_2$.

Fig. 4. Feature comparison between SST and NOMA-SST schemes. This illustration is obtained under a $256 - \Omega$ size SST system with $L = 10$ and SNR $= 10$ dB.

2.3 Properties of NOMA-SST Detection Process

It is noteworthy that NOMA-SST detection process has two major advantages, which are much different from the detection process in frequency domain of pure NOMA systems.

– (i) **No apriori information is required from one user to others**. Note that the SIC procedure subtracts reconstructed content of user with strongest

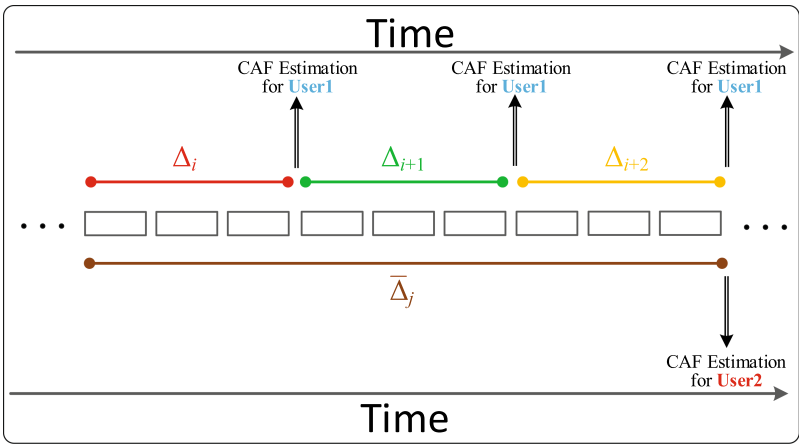

Fig. 5. Detection workflow for NOMA-SST scheme with differential window integration strategy.

power from the mixed signal, and then successively detects the weaker users in a decreasing order of power level. Therefore, a user should at least know the detailed apriori information from users with higher power level than itself, or it cannot obtain its content successfully. However, such a situation is much different in SST domain detection process. According to the workflow (especially the user classification submodule) in the previous subsection, we can find that it is unnecessary for any weaker user to learn the detailed contents of stronger users, only its order of power level is needed.

– (ii) **The error propagation effect is barely involved**. It is widely noticed that there is an error propagation effect [30] existing in frequency domain detection of NOMA systems. Specifically speaking, if the data of stronger users is detected incorrectly, the detection accuracy of the weaker users will be largely hindered. Different from that, the error propagation effect in SST domain detection process is quite slight. Still referring to classification submodule in the previous subsection, we know that even if a stronger user' feature classification goes wrong, the feature classification of a weaker user will hardly be affected. For example, in a $256 - \Omega$ size NOMA-SST system, even if an error detection occurs for the stronger user, the error propagation probability is only 3.9×10^{-3} for the weaker user, which can be neglected in practice.

3 Differential Window Integration Strategy

The previous section has elaborated the operational principle for NOMA-SST technique. However, referring to Fig. 3(b), we notice that the intrinsic power level gaps among NOMA users will inevitably lead to energy gaps among SST

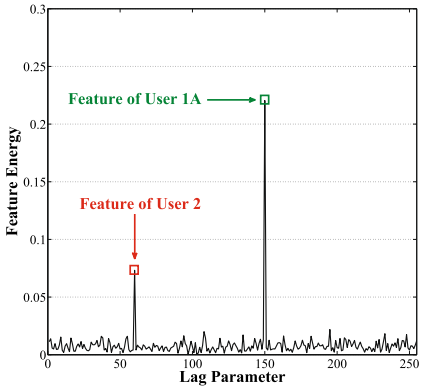

(a) First observation period for User 1.

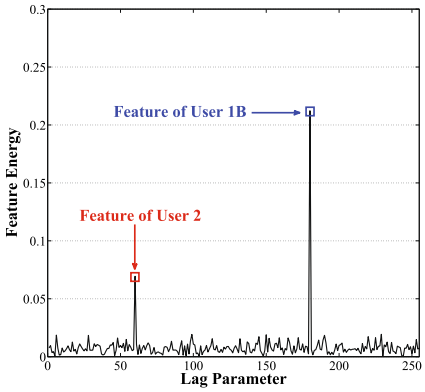

(b) Second observation period for User 1.

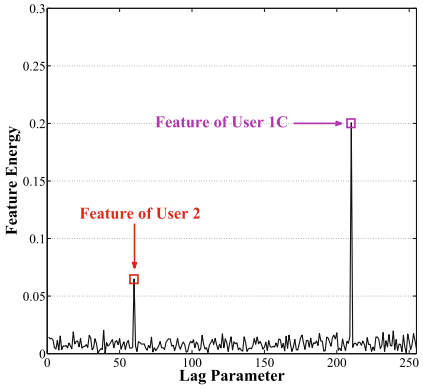

(c) Third observation period for User 1.

Fig. 6. Feature presentation under NOMA-SST scheme with differential window integration strategy: User 1's Perspective. This illustration is obtained under a $256-\Omega$ size SST system with $P_1 = 4P_2$, $L = 10$ and SNR = 10 dB. Here $\bar{\Delta}_j$ is set as 60 for User 2; Δ_i, Δ_{i+1}, Δ_{i+2} are set as 150, 180 and 210 for User 1, respectively. The differential window configuration is User 1: User 2 = 1:3.

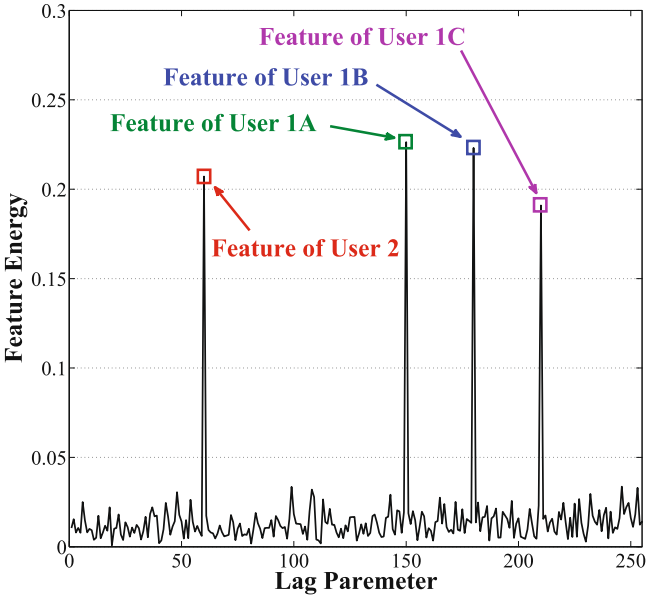

Fig. 7. Feature presentation under NOMA-SST scheme with differential window integration strategy: User 2's Perspective. This illustration is obtained under the exact same situation as that in Fig. 6.

features. Especially under low signal-to-noise ratio (SNR) conditions, the weaker users's SST features are more likely to be inundated by noise. Accordingly, the SST domain detection performance will be quite deviated for different NOMA users.

Confronted with such a circumstance, we dedicatedly design an enhanced transmission strategy for NOMA-SST technique, aiming at compensating SST detection performance for weaker NOMA users. Specifically, the principle is to allocate diverse observation window lengths to different power level users: users with lower power level utilize longer observation window lengths for better accumulations of feature energy; while users with higher power levels retain or decrease the default observation window lengths. The strategy above is named as "Differential Window Integration Strategy".

Figure 5 displays the detection workflow for NOMA-SST scheme with differential window integration strategy. In this example, we use a 3:1 differential window configuration. The higher power user (User 1, occupies Δ_i series) adopts default observation window length L, while the lower power user (User 1, possesses $\bar{\Delta}_j$ series) exploits a wider observation window length $3L$. Since the CAF estimation moments are not synchronized, the detection process here is much different from those of classical SST and default NOMA-SST. Particularly, the feature identification procedure should be divided in two perspective.

Table 1. Simulation parameters.

Parameters	Values
FFT size	128
Cyclic prefix length	32
Channel coding	Convolutional code (5, 7)
Coding rate	1/2
Antenna configuration	2×1
Channel model	Rayleigh fading
Modulation	QPSK
Number of multiplexed NOMA users	2
NOMA mode	Downlink
Proportion of power distribution	Strong user:weak user = 4:1
Default observation window length	10 unit
Differential window configuration	Strong user:weak user = 1:3

- (i) **Perspective of higher power level user**. Figure 6 reveals the feature presentations from User 1's perspective. The three subfigures correspond to the Δ_i, Δ_{i+1} and Δ_{i+2} periods in Fig. 5, respectively. In a User 1's round, it directly calculates the CAF value for past L duration, explores the highest peak from the available feature location range of Ω, and returns the information of the highest peak of Figs. 6(a), 6(b) and 6(c) for Δ_i, Δ_{i+1} and Δ_{i+2}, respectively. The whole identification process above ignores the interference from the weaker power level user since the energy gaps.
- (ii) **Perspective of lower power level user**. Figure 7 shows the feature presentation from User 2's perspective, which corresponds to the $\bar{\Delta}_j$ period in Fig. 5. As we can see in Fig. 7, through the triple-window energy accumulation, User 2's feature energy is comparable to those of User 1's. Direct identification might cause misjudgments. Therefore, the feature identification submodule of User 2's perspective should first collect the identified Δ_i, Δ_{i+1} and Δ_{i+2} from User 1's perspective. Then searches the highest peak from a limit range of $\bar{\Omega} = \Omega - \{\Delta_i, \Delta_{i+1}, \Delta_{i+2}\}$. At last, the peak information is returned to $\bar{\Delta}_j$.

4 Numerical Results

In this section, we evaluate the performance of NOMA-SST technique through numerical analysis. Considering that the frequency domain detection performance of NOMA techniques has been well studied in existing literature, in this section we focus on the SST domain detection performance. The basic simulation parameters are listed in Table 1.

Figure 8 shows the SST domain detection performance of NOMA-SST technique under default mode. It can be observed that the higher power user (User 1,

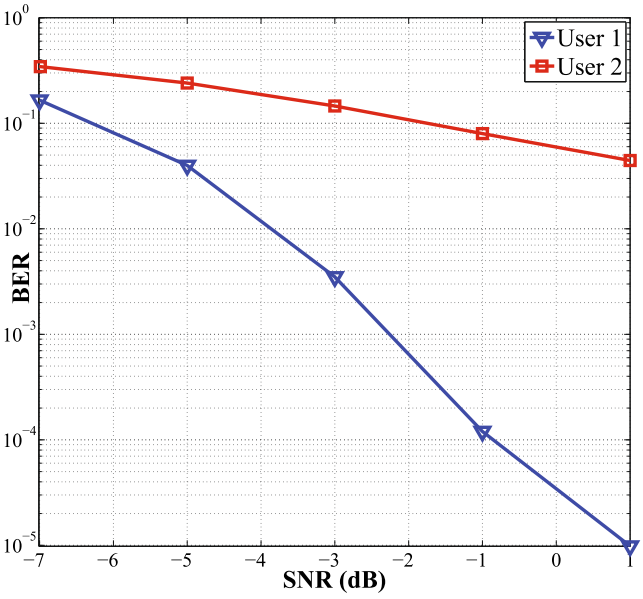

Fig. 8. SST domain detection performance of NOMA-SST under default mode. (Color figure online)

blue curve) achieves an excellent detection performance. It easily gets a bit error rate (BER) of 10^{-5} level after SNR surpasses 0 dB. By contrast, the performance of lower power user (User 2, red curve) is not quite satisfactory. It cannot even reach a 10^{-2} level within the given SNR condition range.

Figure 9 exhibits the detection performance of NOMA-SST technique under differential window integration strategy. Specifically, the differential window configuration is default L for User 1 and triple L for User 2; other system parameters equate to those of Fig. 8. The performances of User 1A, User 1B and User 1C are obtained from anterior, middle and posterior L coverages of User 2's $3L$ observation window, respectively. From the blue, green and purple curves in this figure, we can find two phenomenons: (i) three curves nearly overlap with each other, which reflects that User 1's performance is quite steady under different coverages of User 2's observation window; (ii) User 1's performance in Fig. 9 is very close to that of Fig. 8. This result reveals that differential window integration strategy hardly affects the SST detection performance of higher power user in NOMA system. On the other hand, compared with that in Fig. 8, User 2's performance in Fig. 9 distinctly upgrades by a great order of magnitude: the average gain is about 10 dB throughout the given SNR range of Fig. 8 and Fig. 9, in which the highest gain is 21.7 dB (obtained at SNR = 1 dB). Thus, the effectiveness of differential window integration strategy is verified.

Another interesting phenomenon in Fig. 9 is to find that User 2's performance slightly outperforms those of User 1 at low SNR situations. Note that the differential window configuration is 1:3 for two NOMA users. Theoretically speaking,

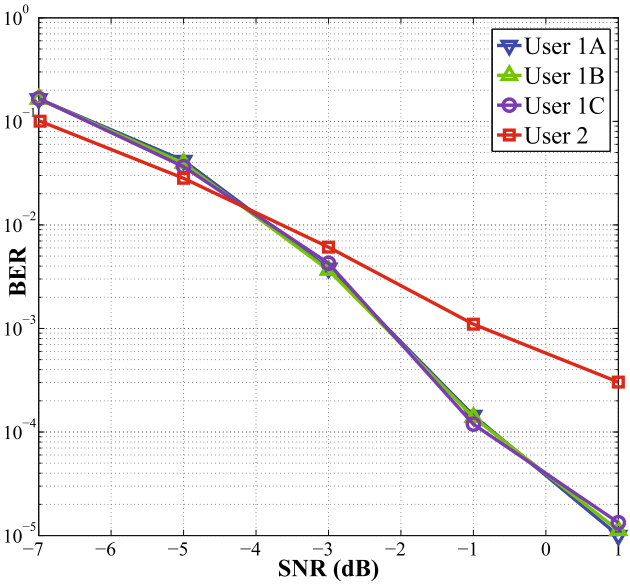

Fig. 9. SST domain detection performance of NOMA-SST under differential window integration strategy. (Color figure online)

such a differential compensation cannot reverse User 2's energy shortage, as the power distribution is 4:1. As such, User 2's performance should be inferior to User 1. Nonetheless, Fig. 9's curve trend at low SNR situations is still reasonable. Because User 2's observation window covers longer time duration than that of User 1. Accordingly, when a sudden adverse channel condition (e.g. deep fading) occurs, User 1's detection performance is easier to be affected; while User 2 has higher possibility to restrain the negative effect, since those sudden adverse channel conditions cannot last long time under power control techniques. Therefore, although the upper bound performance of User 2 is inferior of that of User 1, it is more robust to sudden adverse channel conditions than the latter. This advantage is especially remarkable at low SNR situations.

5 Conclusion

This paper presented a feasible way for integrating NOMA and SST techniques, aiming to seek novel solutions for B5G communications. Specifically, the transceiver architecture, operational workflow and a specialized transmission strategy were successively provided to support the NOMA-SST technique. Numerical results demonstrated that the proposed technique has satisfactory detection performance, which is able to be further enhanced by implementing the add-on differential window integration strategy.

Continuing from the initial research outlined in this paper, future work will be undertaken to further study relationship between user power level gap versus SST detection performance in both uplink and downlink scenarios.

Acknowledgement. The authors' work was supported in part by the Science and Technology Commission Foundation of Shanghai (No. 21511101400), Shanghai Rising-Star Program (No. 21QC1400800), Program of Shanghai Academic/Technology Research Leader (No. 21XD1433700), the National Natural Science Foundation of China (No. 61801460) and the Youth Innovation Promotion Association of CAS.

References

1. Ge, X., Zhou, R., Li, Q.: 5G NFV-based tactile internet for mission-critical IoT services. IEEE Internet Things J. **7**(7), 6150–6163 (2020)
2. Shah, S.A.A., Ahmed, E., Imran, M., Zeadally, S.: 5G for vehicular communications. IEEE Commun. Mag. **56**(1), 111–117 (2018)
3. Xu, T., Zhou, T., Tian, J., Sang, J., Hu, H.: Intelligent spectrum sensing: when reinforcement learning meets automatic repeat sensing in 5G communications. IEEE Wirel. Commun. **27**(1), 46–53 (2020)
4. Aldubaikhy, K., Wu, W., Zhang, N., Cheng, N., Shen, X.: MMWave IEEE 802.11ay for 5G fixed wireless access. IEEE Wirel. Commun. **27**(2), 88–95 (2020)
5. Hassan, N., Yau, K.A., Wu, C.: Edge computing in 5G: a review. IEEE Access **7**, 127276–127289 (2019)
6. Sekander, S., Tabassum, H., Hossain, E.: Multi-tier drone architecture for 5G/B5G cellular networks: challenges, trends, and prospects. IEEE Commun. Mag. **56**(3), 96–103 (2018)
7. Chien, W.-C., Cho, H.-H., Lai, C.-F., Tseng, F.-H., Chao, H.-C.: Intelligent architecture for mobile HetNet in B5G. IEEE Netw. **33**(3), 34–41 (2019)
8. Qi, Q., Chen, X., Lei, L., Zhong, C., Zhang, Z.: Outage-constrained robust design for sustainable B5G cellular Internet of Things. IEEE Trans. Wirel. Commun. **18**(12), 5780–5790 (2019)
9. Zhou, L., Wu, D., Wei, X., Dong, Z.: Seeing isn't believing: QoE evaluation for privacy-aware users. IEEE J. Sel. Areas Commun. **37**(7), 1656–1665 (2019)
10. Jia, R., Chen, X., Qi, Q., Lin, H.: Massive beam-division multiple access for B5G cellular Internet of Things. IEEE Internet Things J. **7**(3), 2386–2396 (2020)
11. Cui, Q., Ni, W., Li, S., Zhao, B., Liu, R.P., Zhang, P.: Learning-assisted clustered access of 5G/B5G networks to unlicensed spectrum. IEEE Wirel. Commun. **27**(1), 31–37 (2020)
12. Vuojala, H., et al.: Spectrum access options for vertical network service providers in 5G. Telecommun. Policy **44**(4), 1–15 (2020)
13. Sakib, S., Tazrin, T., Fouda, M.M., Fadlullah, Z.M., Nasser, N.: An efficient and lightweight predictive channel assignment scheme for multiband B5G-enabled massive IoT: a deep learning approach. IEEE Internet Things J. **8**(7), 5285–5297 (2021)
14. Chen, X., et al.: Age of information aware radio resource management in vehicular networks: a proactive deep reinforcement learning perspective. IEEE Trans. Wirel. Commun. **19**(4), 2268–2281 (2020)
15. Zhou, P., et al.: Edge-facilitated augmented vision in vehicle-to-everything networks. IEEE Trans. Veh. Technol. **69**(10), 12187–12201 (2020)

16. Wang, G., et al.: Coexistence analysis of D2D-unlicensed and Wi-Fi communications. Wirel. Commun. Mob. Comput. **2021**, 1–11 (2021)
17. Zhu, L., Xiao, Z., Xia, X., Wu, D.O.: Millimeter-wave communications with non-orthogonal multiple access for B5G/6G. IEEE Access **7**, 116123–116132 (2019)
18. Li, C., Gao, Z., Xia, J., Deng, D., Fan, L.: Cache-enabled physical-layer secure game against smart UAV-assisted attacks in B5G NOMA networks. EURASIP J. Wirel. Commun. Netw. **2020**(7), 1–9 (2020). https://doi.org/10.1186/s13638-019-1595-x
19. Tusha, A., Dogan, S., Arslan, H.: A hybrid downlink NOMA with OFDM and OFDM-IM for beyond 5G wireless networks. IEEE Sig. Process. Lett. **27**, 491–495 (2020)
20. Zhang, J., Tao, X., Wu, H., Zhang, N., Zhang, X.: Deep reinforcement learning for throughput improvement of the uplink grant-free NOMA system. IEEE Internet Things J. **7**(7), 6369–6379 (2020)
21. Maraqa, O., Rajasekaran, A.S., Al-Ahmadi, S., Yanikomeroglu, H., Sait, S.M.: A survey of rate-optimal power domain NOMA with enabling technologies of future wireless networks. IEEE Commun. Surv. Tutor. **22**(4), 2192–2235 (2020)
22. Wei, F., Zhou, T., Xu, T., Hu, H.: Modeling and analysis on two-way relay networks: a joint mechanism using NOMA and network coding. IEEE Access **7**, 152679–152689 (2019)
23. Napolitano, A.: Cyclostationarity: new trends and applications. Sig. Process. **120**, 385–408 (2016)
24. Wang, X., Zhou, T., Xu, T., Feng, S., Hu, H., Jin, Y.: Fragmental weight-conservation combining scheme for statistical signal transmissions under fast time-varying channels. China Commun. **17**(1), 118–128 (2020)
25. Patra, A.N., Regis, P.A., Sengupta, S.: Distributed allocation and dynamic reassignment of channels in UAV networks for wireless coverage. Pervasive Mob. Comput. **54**, 58–70 (2019)
26. Xu, T., Zhang, M., Hu, H.: Harmonious coexistence of heterogeneous wireless networks in unlicensed bands: solutions from the statistical signal transmission technique. IEEE Veh. Technol. Mag. **14**(2), 61–69 (2019)
27. Chung, K.: NOMA for correlated information sources in 5G systems. IEEE Commun. Lett. **25**(2), 422–426 (2021)
28. Yin, Y., Peng, Y., Liu, M., Yang, J., Gui, G.: Dynamic user grouping-based NOMA over Rayleigh fading channels. IEEE Access **7**, 110964–110971 (2019)
29. Liu, X., Zhai, X.B., Lu, W., Wu, C.: QoS-guarantee resource allocation for multibeam satellite industrial Internet of Things with NOMA. IEEE Trans. Ind. Inform. **17**(3), 2052–2061 (2021)
30. Zhang, H., Zhang, H., Liu, W., Long, K., Dong, J., Leung, V.C.M.: Energy efficient user clustering, hybrid precoding and power optimization in terahertz MIMO-NOMA systems. IEEE J. Sel. Areas Commun. **38**(9), 2074–2085 (2020)
31. 3rd Generation Partnership Project (3GPP); Technical Specification Group Radio Access Network; Evolved Universal Terrestrial Radio Access (E-UTRA); Physical Channels and Modulation (Release 15), 3GPP TS 36.211 V15.1.0 (2018)
32. Iradukunda, N., Nguyen, H.T., Hwang, W.: On cyclic delay diversity-based single-carrier scheme in spectrum sharing systems. IEEE Commun. Lett. **23**(6), 1069–1072 (2019)
33. Kim, K.J., Liu, H., Wen, M., Orlik, P.V., Poor, H.V.: Secrecy performance analysis of distributed asynchronous cyclic delay diversity-based cooperative single carrier systems. IEEE Trans. Commun. **68**(5), 2680–2694 (2020)

34. Axell, E., Leus, G., Larsson, E.G., Poor, H.V.: Spectrum sensing for cognitive radio: state-of-the-art and recent advances. IEEE Sig. Process. Mag. **29**(3), 101–116 (2012)
35. Sun, H., Yuan, S., Luo, Y.: Cyclic spectral analysis of vibration signals for centrifugal pump fault characterization. IEEE Sens. J. **18**(7), 2925–2933 (2018)
36. Camara, T.V.R.O., Lima, A.D.L., Lima, B.M.M., Fontes, A.I.R., Martins, A.D.M., Silveira, L.F.Q.: Automatic modulation classification architectures based on cyclostationary features in impulsive environments. IEEE Access **7**, 138512–138527 (2019)